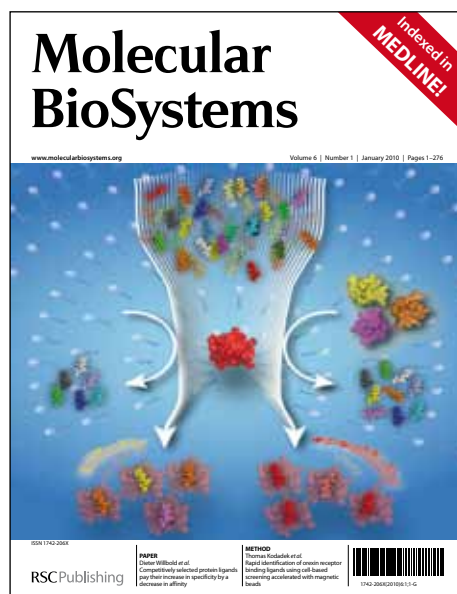


Molecular Biosystems

Accepted Manuscript



This is an *Accepted Manuscript*, which has been through the RSC Publishing peer review process and has been accepted for publication.

Accepted Manuscripts are published online shortly after acceptance, which is prior to technical editing, formatting and proof reading. This free service from RSC Publishing allows authors to make their results available to the community, in citable form, before publication of the edited article. This *Accepted Manuscript* will be replaced by the edited and formatted *Advance Article* as soon as this is available.

To cite this manuscript please use its permanent Digital Object Identifier (DOI®), which is identical for all formats of publication.

More information about *Accepted Manuscripts* can be found in the [Information for Authors](#).

Please note that technical editing may introduce minor changes to the text and/or graphics contained in the manuscript submitted by the author(s) which may alter content, and that the standard [Terms & Conditions](#) and the [ethical guidelines](#) that apply to the journal are still applicable. In no event shall the RSC be held responsible for any errors or omissions in these *Accepted Manuscript* manuscripts or any consequences arising from the use of any information contained in them.

Exploring a Structural Protein-Drug Interactome for New Therapeutics in Lung Cancer

Xiaodong Peng^{3,8}, Fang Wang¹, Liwei Li,^{1,3} Khuchtumur Bum-Erdene,^{1,3} David Xu³, Bo Wang^{1,14} Tony Sinn,^{10,11} Karen Pollok,^{10,11} George Sandusky,¹³ Lang Li,^{3,9,12} John Turchi,¹⁴ Shadia I. Jalal,¹⁴ and Samy Meroueh^{1,4,7,9,11}

¹Department of Biochemistry and Molecular Biology, ²Department of Pharmacology and Toxicology, ³Center for Computational Biology and Bioinformatics, ⁴Stark Neuroscience Research Institute, ⁵Indiana University Cancer Center, ⁶Department of Medicine, ⁸Regenstrief Institute, Inc., ⁹Department of Medical and Molecular Genetics, ¹⁰Herman B Wells Center for Pediatric Research, ¹¹In vivo Therapeutics Core, ¹²Department of Biostatistics, Indiana University School of Medicine, ¹³Department of Pathology and Laboratory Medicine, ¹⁴Department of Medicine, Indianapolis, IN 46202, ¹⁵Department of Chemistry and Chemical Biology, Indiana University Purdue University Indianapolis (IUPUI), Indianapolis, Indiana, 46202.

E-mail: smeroueh@iupui.edu

RECEIVED DATE (to be automatically inserted after your manuscript is accepted if required according to the journal that you are submitting your paper to)

ABSTRACT

The pharmacology of drugs is often defined by more than one protein target. This property can be exploited to use approved drugs to uncover new targets and signaling pathways in cancer. Towards enabling a rational approach to uncover new targets, we expand a structural protein-ligand interactome (<http://www.biodrugscreen.org>) by scoring the interaction among 1,000 FDA-approved drugs docked to 2,500 pockets on protein structures of the human genome. This afforded a drug-target network whose properties compared favorably with previous networks constructed with experimental data. Among drugs with highest degree and betweenness two are cancer drugs and one is currently used for treatment of lung cancer. Comparison of predicted cancer and non-cancer targets reveals that the most cancer-specific compounds were also the most selective compounds. Analysis of compound flexibility, hydrophobicity, and size showed that the most selective compounds were low molecular weight fragment-like heterocycles. We use a previously-developed screening approach using the cancer drug erlotinib as a template to screen other approved drugs that mimic its properties. Among the top 12 ranking candidates, four are cancer drugs, two of them kinase inhibitors (like erlotinib). Cellular studies using non-small cell lung cancer (NSCLC) cells revealed that several drugs inhibited lung cancer cell proliferation. We mined patient records at the Regenstrief Medical Record System to explore possible association of exposure to three of these drugs with occurrence of lung cancer. Preliminary *in vivo* studies using non-small cell lung cancer (NCLSC) xenograft model showed that losartan- and astemizole-treated mice had tumors that weighed 50 ($p < 0.01$) and 15 ($p < 0.01$) percent less than vehicle. These results set the stage for further exploration of these drugs and to uncover new drugs for lung cancer.

INTRODUCTION

Genomic and proteomic studies have established that cancer is a systems biology disease that involves a large number of genes spanning multiple signaling pathways as shown in lung,¹ pancreatic,² breast,³ brain⁴ and colorectal⁵ cancers. In the case of lung cancer, hundreds of genetic alterations spanning 18 signaling pathways have been found.^{1,6} The large number of mutations make it a significant challenge to identify effective treatments for this disease. According to the American Cancer Society, the disease has taken 160,340 lives in the U.S in 2011 alone. Non-small cell lung cancer (NSCLC) is the most prevalent form of the disease (85 percent of all cases). It is characterized by poor prognosis and aggressive behavior. First-line treatment options for the majority of patients include chemotherapeutics that cause significant side effects. New treatments with lower toxicity and greater efficacy are urgently needed.

Studies have shown that approved and experimental drugs as well as chemical probes bind and modulate the function of multiple proteins.^{7, 8} This property, also known as polypharmacology, offers an opportunity to uncover new targets. Recently, we have explored the possibility of using structure-based docking to generate a protein-compound interactome that can be used as a hypothesis generation tool to uncover new targets for small molecules. We docked more than 1,200 compounds to more than 3,000 pockets from 1,000 proteins. The resulting structural protein-ligand interactome (SPLINTER) is available at <http://www.biodrugscreen.org>⁹. The scoring of protein-compound interactions in this interactome enables the rank-ordering of compounds for individual targets for purposes of hit identification, but also makes it possible to rank-order proteins for a list of potential targets for a compound or drug of interest. In a recent application, we used the interactome to search for compounds that mimicked the binding profile of an existing drug.¹⁰ We stipulated that such compounds may exhibit similar pharmacokinetic properties and efficacy to the drug and possibly serve as leads for the development of cancer therapeutics. From this study, several

compounds were uncovered with potent anti-cancer properties and *in vitro* studies suggested suitable pharmacokinetic (PK) properties.¹⁰

Here, we extend SPLINTER by docking more than 1,000 FDA-approved drugs to targets in the interactome. The cancer drug erlotinib was used as a template to search for other approved drugs that may possess similar anti-cancer properties. Erlotinib is used in the treatment of non-small cell lung cancer (NSCLC) patients. Twelve drugs are tested for their effect on cell growth in a panel of NSCLC cells. We mined patient records to study the potential association between drug exposure and lung cancer occurrence in patients taking these drugs.¹¹ *In vivo* preclinical studies using human NSCLC xenografts in NOD-SCID mice were carried out to probe these drugs for their effect in lung cancer.

RESULTS AND DISCUSSION

Docking approved drugs to the human structural proteome. The solvent-accessible surface area (SASA) and volume were determined for each pocket to provide insight into their physico-chemical properties (Fig. 1). The SASA and volume define the shape and size of the pocket. The mean SASA for cancer and non-cancer targets is 367.6 and 353.5 Å² respectively (Fig. 1A and 1G). To put this number in perspective, a typical SASA for a protein-protein interaction is at least 1000 Å² while enzyme active site pockets are smaller. More than 90 percent of the pockets fall within 680 Å². These cavities are located either at protein-protein interaction interfaces, enzyme active sites, or allosteric sites. The mean volume for the cavities is 1029.6 Å³ for cancer targets and 1061.4 Å³ for non-cancer targets (Fig. 1D and 1J). 90 percent of the targets have cavities with volumes that are within 1995 Å³.

To get insight into the physico-chemical properties of binding cavities within the cancer and druggable targets, we defined pseudocenters in the binding pockets following the approach of Klebe and coworkers.¹² These pseudocenters consisted of aromatic, aliphatic, hydrogen bond donors, and acceptors as shown in Fig. 1. On average, there are 13.8 and 14.6 aromatic pseudocenters in the binding cavities of the proteome for cancer and non-cancer targets (Fig 1B and 1H). We found on average 21.1 and 22.7 aliphatic pseudocenters for cancer and non-cancer targets (Fig. 1E and 1K). Hydrogen bond donor and acceptor reflect hydrogen bonding capacity of residues within the binding cavities. The average number of acceptors was 19.7 and 17.3 for cancer and non-cancer targets (Fig. 1C and 1I). The mean number of donors was 17.3 and 14.6 for cancer non-cancer targets (Fig. 1F and 1L).

Physico-chemical properties and polypharmacology. Flexibility and solubility are investigated for approved drugs, approved cancer drugs, and publicly-available NCI compounds. Flexibility is represented by the number of rotatable bonds. Using a threshold

value of 0.1 μM , the number of targets for all three classes versus the size of the small molecule is provided in Fig. 2A. The most promiscuous compounds have about 5 rotatable bonds. The most selective compounds had less than 3 rotatable bonds. High promiscuity is predicted even for compounds with more than 10 rotatable bonds (Fig. 2B). In fact, some drugs with 20 rotatable bonds had more than 1,000 predicted targets at the 0.1 μM threshold. Approved cancer drugs followed a similar pattern. Rotatable bonds for NCI compounds, non-cancer drugs and cancer drugs showed different distributions (Fig. 2B). A significantly greater fraction of NCI compounds had 3-5 rotatable bonds compared with drugs and non-cancer drugs. Rotatable bonds were more uniformly distributed among approved drugs. A significant fraction of drugs and approved drugs had more than 7 rotatable bonds in significant contrast to NCI compounds. Cancer drugs were even more likely to have more than 7 rotatable bond than non-cancer drugs.

It has been suggested that hydrophobic compounds are more promiscuous.¹³ Lipophilicity is quantified by the partition coefficient that corresponds to the ratio of the concentration of compound in water versus n-octanol. Several algorithms have been developed to predict the logarithm of the partition coefficient (cLogP).¹⁴ A plot of the number of pockets versus cLogP for all three classes of compounds shows a gradual increase in promiscuity for compounds with increasing cLogP (Fig. 2C). This is observed for approved non-cancer drugs, approved cancer drugs, and NCI compounds. The mean cLogP was 2.3, 2.7 and 2.5 for the three classes of compounds, suggesting that cancer drugs had slightly more hydrophobic character than other drugs and compounds. This is illustrated by the distribution in Fig. 2D as a greater proportion of cancer drugs had cLogP values greater than 5. The distribution also shows that compounds from the NCI library were more likely to have a cLogP between 1 and 3.

Drug pharmacology. Compounds that bind selectively to cancer-associated targets are more desirable as they are likely to possess greater efficacy and lower toxicity. To get insight into the selectivity of drugs, the Cancer Selectivity Index (CSI) is defined as the ratio of the

number of predicted cancer target proteins from the HCPIN database to predicted non-cancer targets of approved drugs obtained from DrugBank. A plot of *CSI* versus the total number of predicted targets (HCPIN + DrugBank) for each drug is shown in Fig. 2E. A protein is considered a “target” when the predicted binding affinity from the ChemScore empirical scoring function exceeds a predefined threshold of 0.1 μM . ChemScore has been extensively validated for scoring protein-compound complexes.^{15, 16} For the majority of drugs, the *CSI* ratio is in the 0.7 to 1.2 range. This is not completely unexpected since pockets located on cancer targets are similar to those located on non-cancer targets. A close inspection of the data reveals that there were 500 drugs with *CSI* greater than 1. A significant proportion among them, 64 are approved cancer drugs. Twelve of these have a high degree of preference to cancer targets with *CSI* values greater than 2 (Table 1). All twelve had a total of less than 18 targets (that exceeded the 0.1 μM threshold). Their chemical structure is provided in Supporting Information Fig. S1. It was notable that the overwhelming majority of these drugs were fragment-like with molecular weights below 300 Da. They consisted of a single heterocyclic or aromatic ring structure with various appendages. This suggests that smaller compounds may be the most effective approach to achieve selective polypharmacology.

A measure of the predicted polypharmacology of compounds was defined using the ratio of targets defined by the number of proteins that exceeded the 0.1 μM threshold to the number of proteins below this threshold. The distribution of this ratio is shown in Fig. 2F. The majority of NCI compounds and drugs exhibit a ratio below 0.2, with compounds showing greater selectivity than drugs. Cancer drugs exhibit less selectivity than NCI compounds and non-cancer drugs (Fig. 2F).

A survey of the literature reveals that at least four of these drugs bind to targets that have previously been implicated in cancer. For example, isoetharine and salbutamol are adrenergic β_1 , β_2 agonists and are used for the treatment of bronchospasm, asthma, and

chronic obstructive pulmonary disease. They bind and activate the β 1 and β 2 adrenergic receptors, which are involved in multiple metabolism pathways including calcium signaling, gap junction, salivary secretion, and endocytosis.¹⁷ Recent studies suggest these receptors are critical for the development of colorectal cancer.¹⁸ The third drug is methyprylon, a sedative of the piperidinedione derivative family and a treatment for insomnia. Up-regulation of microRNA miR-155 inhibits γ -aminobutyric acid A receptor 1 (GABRA1, target of methyprylon) and promotes tumor growth.¹⁹ The targets of the fourth drug (bromfenac) are cox1 and cox2, which are well-known to be involved in inflammation, which in turn has been implicated in cancer.²⁰

Drug-target network. The interaction between small molecules and their targets can be understood within the context of a drug-target network.^{8, 21} The availability of complete protein-drug or protein-compound interactome affords the construction of a complete drug-target network (Fig. 3). In this network, a node represents a molecule and two nodes are linked if they share a cancer target. A protein is considered a target to a small molecule if its ChemScore predicted affinity is higher than 0.01 μ M. We constructed a drug network for cancer and non-cancer FDA-approved drugs (Fig. 3A).

A comparison of the two networks reveals a total of 120,314 and 54,632 edges, with 559 and 402 nodes for the NCI compounds and FDA-approved drugs, respectively. To gain insight into the level of interconnections of the nodes, we computed the mean degree for each network (the degree of a node corresponds to the number of edges connected to the node). The NCI compound network exhibited a mean degree of 430, while the FDA-approved drug network showed a mean degree of 272. The number of non-redundant shortest pathways going through each node (betweenness) was also computed for each network. The mean betweenness for the NCI network was 128 while that of the FDA-approved drug network was 131. A plot of the degree versus betweenness is shown in Fig. 3B. The top 10 drugs with highest betweenness and degree are provided in Table 2. *It is worth noting that two of the ten compounds are cancer*

drugs, and one, namely bexarotene, is used in the treatment of lung cancer (Table 2).²² Finally, the mean clustering coefficient was determined to gain insight into the topology of the networks. Clustering coefficient of the NCI compound network is 0.913 while that of the FDA-approved drug network is 0.898. It was found that the NCI compound network was slightly less loosely connected than the FDA-approved drug network. These values are in excellent agreement with a previous study that computed them from a drug-network based on experimental data.²³

A search for new cancer drugs using compound polypharmacology. Previously, we had used predicted off-targets of erlotinib to identify compounds that mimicked the pharmacokinetic and anti-cancer properties of the cancer drug. Here, we extend this concept to identify FDA-approved drugs that could be potentially used in the treatment of lung cancer. Following the same approach a fingerprint is defined based on erlotinib's predicted off-targets.¹⁰ We selected the top 12 drugs with highest similarity to the binding profile of erlotinib as measured by a Tanimoto coefficient that was determined by comparing fingerprints (Table 3). *It was notable that among these 12 drugs, 4 are either currently used for the treatment of cancer, or have been considered in clinical trials as candidates for the treatment of cancer; these include lapatinib, dasatinib, bexarotene, and podofilox.* Lapatinib is approved for advanced or metastatic breast cancer. Dasatinib is approved BCR-ABL positive chronic myelogenous leukemia. Bexarotene is approved for treatment of T-cell lymphoma and is being studied in a Phase II lung cancer clinical trial. All of these drugs were tested in clinical trials for treatment of lung cancer. Podophyllotoxin (podofilox) is approved to treat external genital warts; due to its tubulin modulation property and antimitotic function, podophyllotoxin and its derivatives may have anticancer properties.²⁴ Another significant outcome of the ranking by fingerprint using erlotinib is the fact that two of the anti-cancer drugs, namely lapatinib and dasatinib, are kinase inhibitors just like erlotinib. *The most significant aspect of this observation is that the fingerprint approach can be used to identify other drugs that target the same protein as the template drug*

without the use of chemical structure. It is interesting to note that none of the drugs shared any structural similarity with erlotinib. Hence, our fingerprint approach obviates the need to use chemical structure to identify pairs of small molecules that share similar targets.

In an effort to assess the effect of each drug on cancer cell growth, we performed an MTT study for each drug in three NSCLC cancer cell lines, namely H1299, A459, H460, and one non-cancer WI38 fibroblast cell line. All 32 MTT curves are provided in the Supporting Information Fig. S1 to S4. EC_{50} that were obtained from these curves are provided in Table 4. The most cytotoxic drug was podophyllotoxin with EC_{50} in the nanomolar concentrations (Table 4). This was not a surprising finding since this drug is a derivative of etoposide a well-known chemotherapeutic. The second most potent drug was dasatinib. In A549 and WI38, the compound inhibited proliferation at sub-micromolar EC_{50} . Astemizole was the next most cytotoxic drug, EC_{50} of 12, 9, 10, and 8 μM for H1299, H460, A549 and WI38 cells, respectively. Lapatinib, another kinase inhibitor, showed significantly less inhibition of cell proliferation in all three cell lines with EC_{50} values between 30 to 40 μM . Bexarotene, which was previously tested in lung cancer clinical trials revealed weaker anti-proliferative effect ($EC_{50} = \sim 50 \mu\text{M}$), showed weaker effect on WI38 proliferation. Ergotamine, an analog of dihydroergotamine, had higher potency with an $EC_{50} \sim 25 \mu\text{M}$ in H1299 and H460, and even greater potency in A549 cells (13 μM). What sets this compound apart from the others is that it had significantly less effect on WI38, providing a potential therapeutic window. Losartan, a drug used mainly to treat high blood pressure, showed very little cytotoxicity even at concentrations up to 100 μM .

Mining and statistical analysis of clinical drug exposure and disease occurrence.

Patient cohorts were defined based on different drugs. For losartan, patient cohort was constructed as co-occurrence of hypertension prior to lung cancer plus mono-occurrence of hypertension without any kind of cancer. For ergotamine, patient cohort was constructed as co-occurrence of migraine pain prior to 12 major types of cancer (Supporting Information Table S1)

plus mono-occurrence of migraine pain without any kind of cancer. All cohorts contained patients who had first diagnosis of hypertension or migraine pain at 30 years of age or older. We extracted 67,109 patients in the losartan/hypertension cohort, among which 65,411 patients had not been exposed to losartan and 1,698 patients had been exposed to losartan before first diagnosis of lung cancer or last visit date; and among which 1,574 patients were diagnosed with lung cancer sometime after first hypertension diagnosis and 65,535 patients were not diagnosed with any cancer before last visit date (Table 5). For ergotamine/migraine pain cohort, we extracted 44,721 patients in the ergotamine/migraine pain cohort, among which 44,509 patients had not been to ergotamine and 212 patients had been treated with ergotamine before first diagnosis of any of major cancer types; and among which 1,171 patients were diagnosed with any of 12 major cancers after first migraine pain diagnosis and 43,550 patients were not diagnosed with any cancer before last visit date (Table 6).

Survival statistical analysis was conducted for the association of drug exposure and risk of cancer (Fig. 4). Time to occurrence of cancer by drug exposure status was analyzed using the Kaplan-Meier method and log-rank test. Survival time (time to occurrence of cancer) was defined as the time from the date of first diagnosis of hypertension (for losartan) or migraine pain (for ergotamine) until date of first diagnosis of lung cancer (for losartan) or any of the 12 major cancer types (for ergotamine). Drug exposure status was considered positive if the patient was prescribed the drug before first diagnosis of cancer or last visit date. Patients who did not have cancer were censored until last visit date. The y-axis corresponds to the fraction of patients who had not been diagnosed with cancer. The x-axis corresponds to survival time in days from first diagnosis of hypertension until first diagnosis of lung cancer (for losartan group) (Fig. 4A), and days from first diagnosis of migraine pain until first diagnosis of any of 12 major cancers in the case of ergotamine (Fig. 4B). For losartan (Fig. 4A green curve), survival time was longer than without losartan (Fig. 4A red curve) at any cancer percentage in range. While with ergotamine (Fig. 4B green curve), survival time was shorter than without ergotamine (Fig.

4B red curve) at most cancer percentage in range. These conditions suggested further statistical confirmation on association of exposure of losartan and astemizole with reduced and enhanced cancer risk respectively.²⁵

***In vivo* studies in mouse xenograft models.** Astemizole, losartan, and ergotamine were evaluated for their effect *in vivo* on tumor growth using an H460 NSCLC human xenograft model. Two studies were carried out. The first study was done by orally dosing mice with ergotamine at 50 mg/kg orally (n = 7) (Fig. 5A). Vehicle mice (n = 8) were dosed with the methylcellulose. The study was terminated at day 21. While differences in tumor volume in vehicle versus compound-treated mice were not statistically significant, there were some trends worth noting in this early exploratory study. At day 15, tumor volume ranged from 249 to 944 mm³ for ergotamine-treated mice, and 274 to 743 mm³ for vehicle.

Another study was carried out with losartan and astemizole. These drugs were administered i.p. at a dose of 50 and 10 mg/kg daily, respectively (n = 10 for losartan and vehicle; n = 9 for astemizole). Another difference is that mice were dosed with drug for a period of 7 days before tumors were implanted. At day 24, tumor size was measured (Fig. 5B). Tumor volume ranged from 1,770 to 4,600 mm³ for vehicle mice. For treated mice, tumor size ranged from 1271 to 3,773 for losartan, and 1,470 to 3,969 mm³ for astemizole, respectively. The median tumor volume was 2,800, 2,463, and 2,810 for vehicle, losartan, and astemizole, respectively. Tumor weights, which measured on the last day of the study were 50 percent smaller for losartan-treated mice (p<0.01), and 15 percent for mice treated with astemizole (p<0.01) (Fig. 5C). Four of the losartan-treated mice developed tumors that weight less than 2.5 g, compared with none of the vehicle (smallest tumors for vehicle was 3.2 g). Three astemizole treated mice developed tumors that weighed less than 3.2 g. During this study, the animal's body weight was monitored (Supporting Information Fig S5) and no significant alteration was found.

Histopathology studies were performed on the resected lung tumors to evaluate the cell cycle arrest of NSCLC cells. The mitotic index (MI) was measured, which is defined as the ratio of mitotic cell to non-mitotic cells for tumor tissues treated with vehicle, losartan, and astemizole. The results were 7, 18, and 8 respectively. These data seem to suggest that losartan has a significant propensity to cause G₂M arrest in the cell cycle, which may lead to apoptosis, similar to mechanism of Paclitaxel, a microtubule stabilizer and a well-known cancer drug.^{26, 27}

CONCLUSION

We extend our protein-compound interactome SPLINTER by docking FDA-approved drugs to a large set of proteins within the dataset. The scoring of these protein-compound structures using ChemScore led to a predicted binding affinity for each protein-compound pair. The resulting matrix of predicted binding affinities can be used to rank proteins for each drug to identify the most likely targets for that drug, or to rank drugs for individual proteins to identify potential hit compounds. A protein is defined as a target for a drug if its predicted binding affinity exceeds a pre-defined threshold value. This matrix was instrumental to enable us to get deeper insight into the pharmacology of these drugs particularly in cancer. Since our interactome consists of cancer and non-cancer proteins, it was possible to identify drugs that exhibited greater selectivity to cancer targets. The data revealed that selectivity for cancer targets can only be achieved only for compounds with fewer predicted targets overall. In addition, it was possible to study the predicted polypharmacology of compounds and drugs. In general compounds from chemical libraries had greater promiscuity than drugs, but cancer drugs exhibited more promiscuity than non-cancer drugs. In addition, physico-chemical properties of compounds and drugs led to significant differences predicted polypharmacology. The data also revealed that smaller fragment-like compounds exhibited greater selectivity. Finally, protein-compound scores enabled a network analysis and led to the discovery of highly interconnected hubs that may yield new cancer therapeutics among existing FDA-approved drugs. Interestingly, the

parameters of these networks based on predicted binding affinity were in good agreement with previous network constructed on experimentally-determined interactions.

Beyond a deeper understanding of compound pharmacology, the protein-compound score matrix provided an opportunity to extend on previous work that revealed that binding profiles can be used effectively to identify compounds that share similar pharmacology.²⁸ The binding profile of compounds was encapsulated into a fingerprint. We defined these fingerprints as bits of 0 and 1 that correspond to whether the compounds exceeded a pre-defined threshold. In our previous application we used a drug to search commercial libraries for compounds that mimic the properties of that drug.²⁸ Here, we extend this approach to FDA-approved drugs that we have docked to all proteins within our interactome. As we have done previously, we use the lung cancer drug erlotinib as a template and use its fingerprint to search for other approved drugs that share a similar fingerprint with the expectation that these drugs will possess similar pharmacology to erlotinib. The fingerprints are compared using a Tanimoto coefficient as we have done previously.²⁸ From this analysis, the top 12 drugs that possessed the most similar fingerprints as erlotinib were further analyzed. It was interesting that three of these drugs are already in use for treatment of lung and other cancers. Among the remaining nine drugs, cellular studies revealed that except for one case, these drugs were micromolar inhibitors of NSCLC proliferation in a panel of NSCLC that include A549, H1299 and H460.

We selected two drugs (losartan and ergotamine) that are commonly prescribed in the clinic and for which there is extensive clinical data at the Regenstrief Institute database. We were interested in evaluating whether patients that take these drugs are less likely to develop cancer than those that do not. Mining patient records at the Regenstrief Institute, our preliminary results indicate that ergotamine may hasten the onset of cancer; while losartan had the opposite effect. Further statistical analyses and controls are needed in future studies to make a definite link between these drugs and lung cancer in patients. Three drugs were tested in a subcutaneous model of NSCLC in NOD-SCID mice. Mice treated with losartan and astemizole had

tumors that weighed 50% and 15% less than vehicle, respectively. In histopathological analysis of resected lung tumors, losartan induced more significant G₂M arrest in the cell cycle.

MATERIALS AND METHODS

Docking approved drugs structures. Previously, we had docked 1592 compounds from the NCI diversity set to 1918 binding pockets that were found at the surface of protein structures that have been previously implicated in cancer.^{9, 10} In this work, an additional 1084 FDA-approved small molecule drugs obtained from DrugBank²⁹ were docked to 2546 cavities on 1738 proteins following the same process that we described previously.⁹ The strength of the interaction between drug and target was determined using the ChemScore empirical scoring function.

Calculation of physico-chemical properties. The protein targets were collected from two sources: HCPIN³⁰ and DrugBank^{29, 31} databases. The first HCPIN release contained structures up to February of 2006. We created a local updated version of the database. We obtained sequence information for all HCPIN targets at the UniProt Web site (<http://www.uniprot.org>) using the SwissProt name provided by the HCPIN Web site. Proteins without a SwissProt name were not included. DrugBank provided sequence information for all targets of existing approved drugs obtained directly from the DrugBank Web site. In total, we collected 3,155 human sequences, 1,147 and 2,241 corresponded to DrugBank and HCPIN proteins, respectively. Among them, 233 were overlapped between the two databases. A BLAST search was carried against RCSB Protein Data Bank (PDB) proteins to map sequence to structures. The crystal structures were obtained from the PDB. 572 and 1065 PDB structures were identified for DrugBank and HCPIN sequences respectively. Solvents, ligands and binding partners were removed from the crystal structures. The REDUCE program³² was used to add hydrogen atoms to proteins and optimize some of the residue orientations. The MGLTOOLS (v1.5.2)³³ was used to assign Gasteiger charges to the protein and generate a structural file for

docking. The structural files were then processed with RELIBASE+^{34, 35} to detect binding pockets and compute pocket physico-chemical properties, including volume, aromatic pseudocenters, aliphatic pseudocenters, hydrogen bond donor, hydrogen bond acceptor and donor/acceptor. A probe radius of 1.4 Å was used to compute the pocket solvent accessible surface area (SASA). The physico-chemical properties for drugs and compounds, including cLogP and number of rotatable bonds, were computed with the QIKPROP program in the Schrödinger package. The mol2-formatted coordinate files of drugs and NCI diversity compounds were downloaded from DrugBank²⁹ and ZINC.³⁶

Erlotinib binding profile calculation. We used the crystal complex of elotinib bound to EGFR as the reference structure and identified 11 potential targets¹ including EGFR from HCPIN by docking elotinib to HCPIN target crystal structures if available. The targets were selected using a consensus scoring function consisting of ChemScore³⁷ and GoldScore³⁸ implemented in SYBYL program. Complex scored more favorable than the reference structures was considered as a potential target and set an ON bit in the binding profile fingerprint. Hence there are 11 ON bits in case of elotinib, which constitutes the fingerprint of binding. The binding profile of any other FDA-approved small molecules was compared to the elotinib. The similarity was measured by Tanimoto coefficient.³⁹

Cell culture. Human NSCLC cell lines H1299 and H460 cells were cultured in RPMI-1640 medium (Cellgro, Manassas, VA). Human epithelial cell line A549 was cultured in Dulbecco's Modified Eagle Medium (Cellgro, Manassas, VA). Each medium was supplemented with 10% FBS and 1% penicillin/streptomycin in a 5% CO₂ atmosphere at 37 °C.

Proliferation assay. The procedure consisted of culturing cells in 10% FBS-DMEM or RPMI-1640 medium containing various amounts of compounds. 20 mM drug stock in 100% DMSO was serially diluted and added into each well of a 96-well plate. Cells were treated and

incubated for 3 days. Viable cells were quantified by MTT assay at absorbance of 570 and 630 nm.

Mining and statistical analysis of clinical drug exposure and disease occurrence data. Retrospective, observational clinical studies were performed with patient data in the Indiana Network of Patient Care (INPC) database formatted to Common Data Model (CDM) of the Observational Medicine Outcomes Partnership (OMOP), which is an NIH-funded public-private partnership for drug safety surveillance.^{40, 41} INPC is a local health information infrastructure, which is maintained at the Regenstrief Institute. It includes most of the Regenstrief Medical Record System (RMRS) clinical data (660 million separate results) from five major hospital systems (fifteen separate hospitals) of central Indiana, county and state public health departments, Indiana Medicaid, and RxHub.⁴² After INPC was formatted to the CDM format of OMOP, the database contained records of 2002480 distinct persons spanning from January 1, 2003 to December 31, 2009. The data structure of OMOP CDM⁴³ allowed us to retrieve patient data such as demographic data, starting/ending date of multiple episodes of drug exposure, starting date of disease diagnosis, and last visit date with database query language SQL. The extraction of diseases including hypertension, migraine pain and cancers was based on codes in Ninth Revision of International Classification of Disease (ICD-9) adopted by WHO in 1975 (Supporting Information Table S1). We focused on 12 major types of cancer which are among top ten deadly cancers in the U.S. either in male, female, or both for the year of 2008. Statistical analysis and graphing were performed with SAS (9.2), IBM SPSS Statistics 19 and SigmaPlot (11.0).

***In vivo* xenograft studies.** NOD/SCID mice were obtained from the on-site breeding colony maintained by the *In Vivo* Therapeutics Core at the Indiana University Simon Cancer Center (IUSM, Indianapolis, IN). H460 cells (2×10^6) were injected subcutaneously into the right flank of 8-10 week old NOD-SCID mice. These cells were obtained directly from ATCC

(Manassas, VA) and used at low passage (<10). Mice were randomized to treatment group based on average tumor volume (mm^3). Two different studies were conducted. The first consisted of PO dosing of mice with ergotamine (n =7) at a dose of 50 mg/kg or a PBS solvent control (n = 8). Mice were dosed once a day for 14 days. The second study involved three groups: Astemizole, losartan, and PBS control. For this study, prior to tumor implant, the animals were pre-treated with drugs daily for a period of 7 days. Following subcutaneous tumor implantation animals were treated with astemizole and losartan that were administered intraperitoneally at 10 mg/kg, once a day for 28 days, respectively. Tumor growth was measured over time via electronic caliper and volume calculated as $\text{Length} * \text{Width}^2/2$ in millimeters. After four weeks mice were euthanized, the lungs were resected, fixed in formalin solution, sectioned, and stained with hematoxylin and eosin (H&E) for analysis.

ACKNOWLEDGMENTS

The research was supported by the NIH (CA135380 and AA0197461) and the INGEN grant from the Lilly Endowment, Inc. (SOM). We acknowledge Indiana University School of Medicine Lungs for Life fellowship to LL. XP is a recipient of National Library of Medicine Biomedical Informatics Fellowship (LM007117-14). Computer time on the Big Red supercomputer at Indiana University is funded by the National Science Foundation and by Shared University Research grants from IBM, Inc. to Indiana University. We wish to acknowledge Tony Sinn, Jayne Silver and Kacie Peterman and the *In Vivo* Therapeutics Core for their expert technical assistance with the *in vivo* studies.

FIGURE LEGENDS

- Figure 1. Physico-chemical properties of binding pockets on cancer targets and non-cancer targets. (A, G) Solvent-accessible surface area (SASA). (D, J) Volume of the cavities identified in targets. (B, H) Distribution of aromatic; (E, K) aliphatic; (C, I) hydrogen-bond acceptors; and (F, L) hydrogen bond donors within binding pockets.
- Figure 2. Physico-chemical properties of the cancer drugs, non-cancer drugs and non-drug compounds using 0.1 μM binding threshold. (A) Compound rotatable bonds versus number of targets. (B) Distribution of rotatable bonds among NCI compounds, non-cancer and cancer drugs. (C) Logarithm of the partition coefficient (cLogP) vs. number of cavities. (D) Distribution of cLogP among NCI compounds, non-cancer and cancer drugs. (E) Ratio of cancer to non-cancer targets of cancer drugs and non-cancer drugs. (F) Distribution of ratio of targets over non-targets among for NCI compounds, non-cancer drugs, and cancer drugs.
- Figure 3. Drug-target networks for cancer drugs and non-cancer drugs. (A) Overview of drug-target networks. Each node represents a drug and two nodes are linked if they share a target. (B) Degree and betweenness of the drugs. Degree of a node is defined as the number of edges connected to the node. Betweenness of a node is defined as the number of non-redundant shortest pathways going through each node.

Figure 4. Kaplan-Meier time to cancer occurrence curves of patients with (green curve) or without (red curve) losartan (A) and ergotamine (B). Time to cancer occurrence was measured from occurrence of 1st hypertension diagnosis to 1st diagnosis of lung cancer (A) and from occurrence of 1st migraine pain diagnosis to 1st diagnosis of any of the major cancer types (B).

Figure 5. Effects of losartan and astemizole on tumor growth in an H460 NSCLC xenograft mouse model.

Drug Name	Total Cancer targets	Total Approved Drugs targets	CSI	Targets
Isoetharine	4	1	4	β_1 adrenergic receptor
Salbutamol	3	1	3	$\beta_{1,2}$ adrenergic receptor
Guanadrel sulfate	2	1	2	Sodium-dependent noradrenaline transporter
Diatrizoate	4	2	2	N/A
Rimantadine	2	1	2	Influenza A virus matrix protein 2

Table 1 Drugs that Exhibit High Selectivity and Preference to Oncology Targets

Starvudine	2	1	2	HIV1 reverse transcriptase
Phensuximide	2	1	2	N/A
Diethylpropion	8	4	2	Sodium-dependent noradrenaline and dopamine transporters
Bromfenac	12	6	2	COX1, 2
Methyprylon	2	1	2	γ -aminobutyric acid receptor subunit alpha-1
lophendylate	2	1	2	N/A
Methsuximide	10	5	2	Voltage-dependent T-type calcium channel

Table 2. Top FDA-Approved Drugs with the Highest Betweenness and Degree Obtained from a Network Analysis of the Data

Name	Betweenness	Degree	Indication
Tacrine	2027	348	Alzheimer's
Sulfisoxazole	1896	310	Antibacterial
Adapalene	905	376	Acne
Flurbiprofen	786	293	Inflammation and Pain
Naftifine	651	367	Antifungal
Conjugated Estrogens	622	360	-
Nilotinib	593	355	leukemia
Proflavine	590	359	bacteriostatic
Bexarotene	571	374	Cancer including lung
Tolcapone	531	349	Parkinson

Table 3. Top FDA-Approved Drugs Identified using Erlotinib Binding Profile

Name	Indication (DrugBank)
Ergotamine	Migraine headaches
Treprostinil	Pulmonary Arterial Hypertension
Bexarotene	Cutaneous T-cell lymphoma
Astemizole	Seasonal allergic rhinitis
Podofilox	External genital warts (Condyloma acuminatum)
Forasartan	Hypertension
Acenocoumarol	Thromboembolic diseases
Desoxycorticoserone Pivalate	Adrenocortical insufficiency
Dihydroergotamine	Migraine headaches
Latanoprost	Glaucoma or ocular hypertension
Lapatinib	Advanced or metastatic breast cancer
Dasatinib	Chronic, accelerated, or myeloid or lymphoid blast phase chronic myeloid leukemia

Table 4. EC₅₀ Values for 8 Drugs on Lung Cancer Cells

Drug Name	EC ₅₀ (μM)			
	H1299	H460	A549	WI38
Dihydroergotamine	70±9	67±1	43±2	80±24
Astemizole	12±1	9±1	10±1	8±1
Podophyllotoxin	0.003±0.032	0.0002±0.0007	0.024±0.002	-
Ergotamine	252±3	26±1	14±1	57±4
Losartan	-	-	63±7	9±3
Lapatinib	41±2	32±1	67±11	32±1
Dasatinib	-	-	0.1±0.04	0.7±0.4
Bexarotene	44±2	52±2	58±4	76±10

Table 5. Patient Records Data to Assess Effect of Losartan in Cancer

	Lung cancer	No cancer	Total
Losartan	26	1672	1698
No losartan	1548	63863	65411
Total	1574	65535	67109

Table 6 Patient Records Data to Assess Effect of Ergotamine in Cancer

	Any cancer	No cancer	Total
Ergotamine	13	199	212
No ergotamine	1158	43351	44509
Total	1171	43550	44721

Figure 1

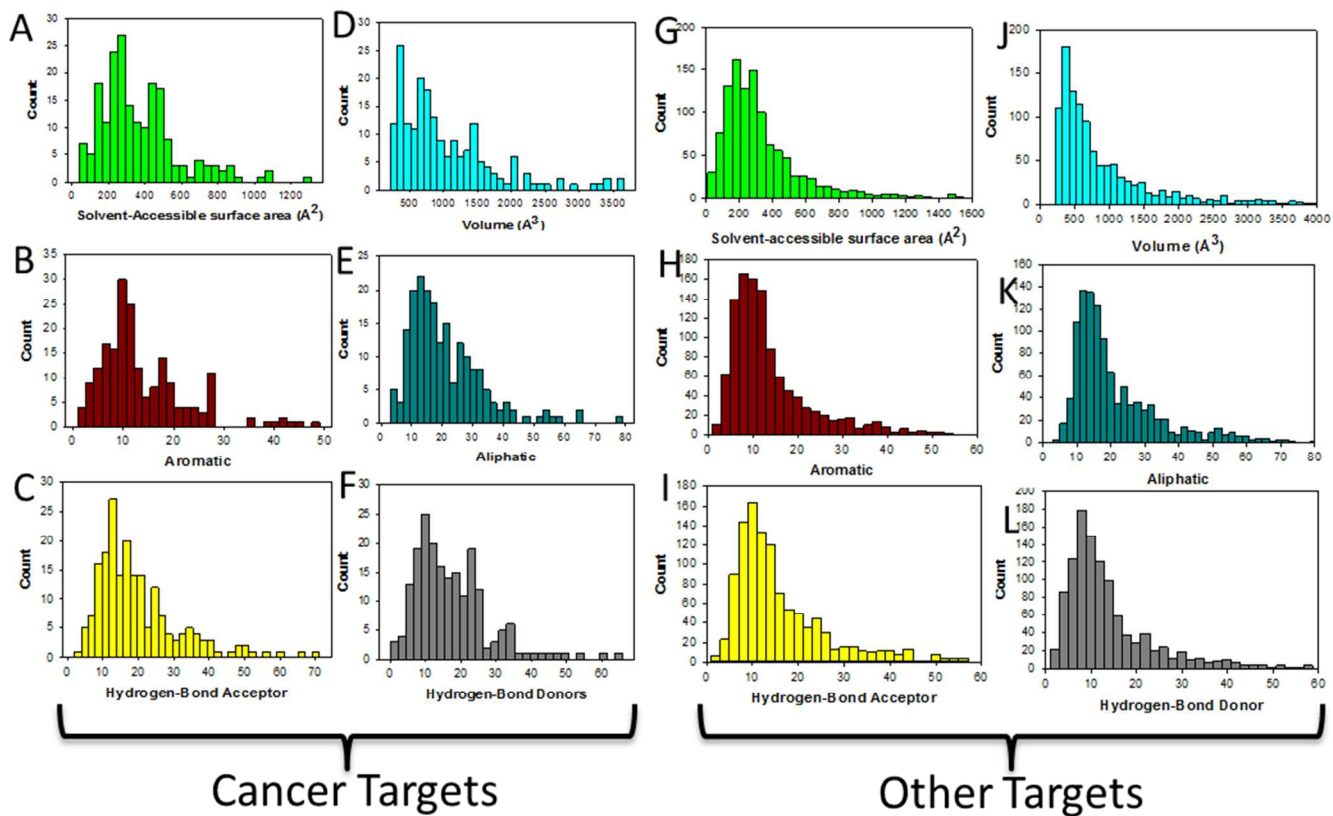


Figure 2

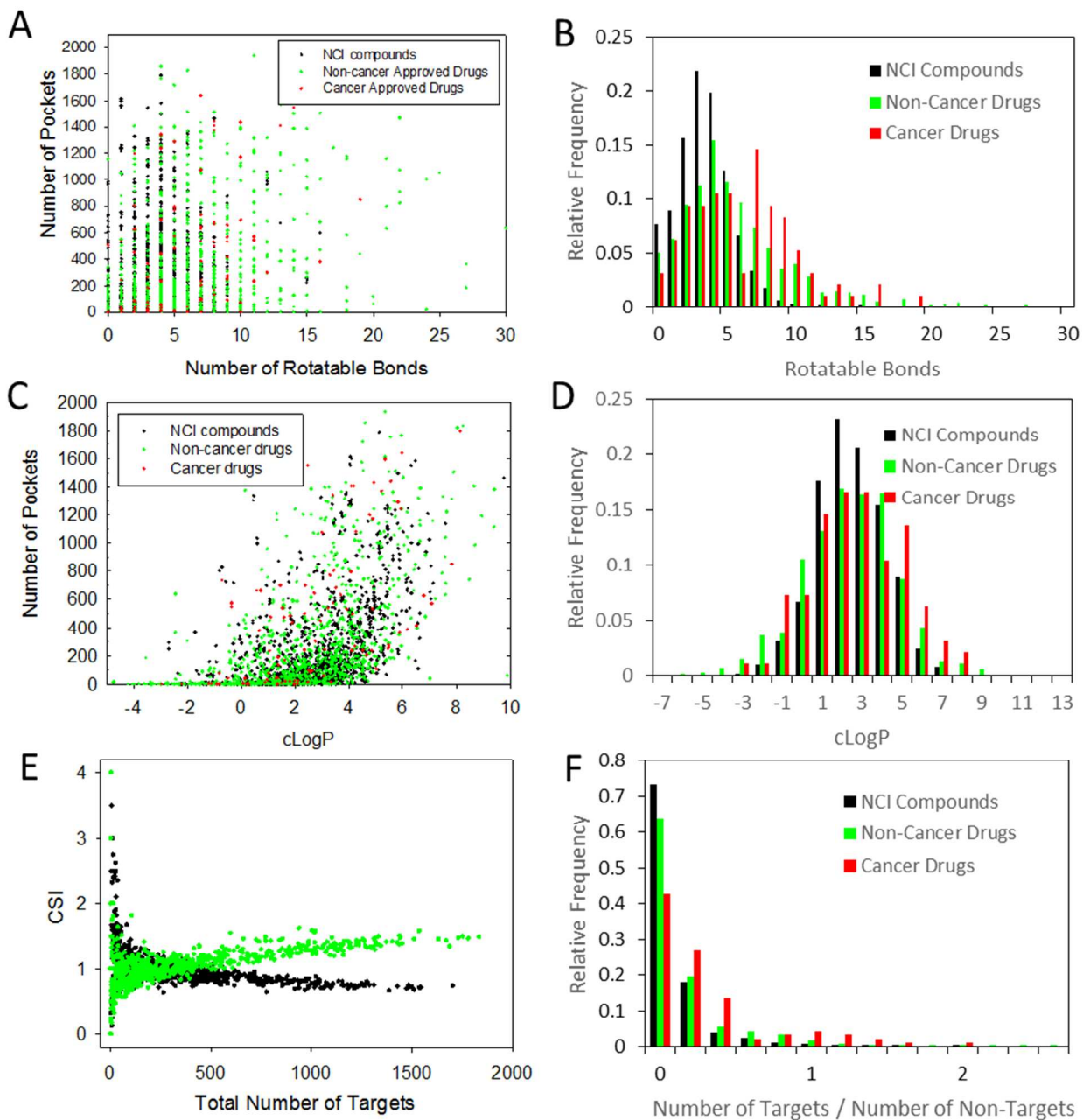


Figure 3

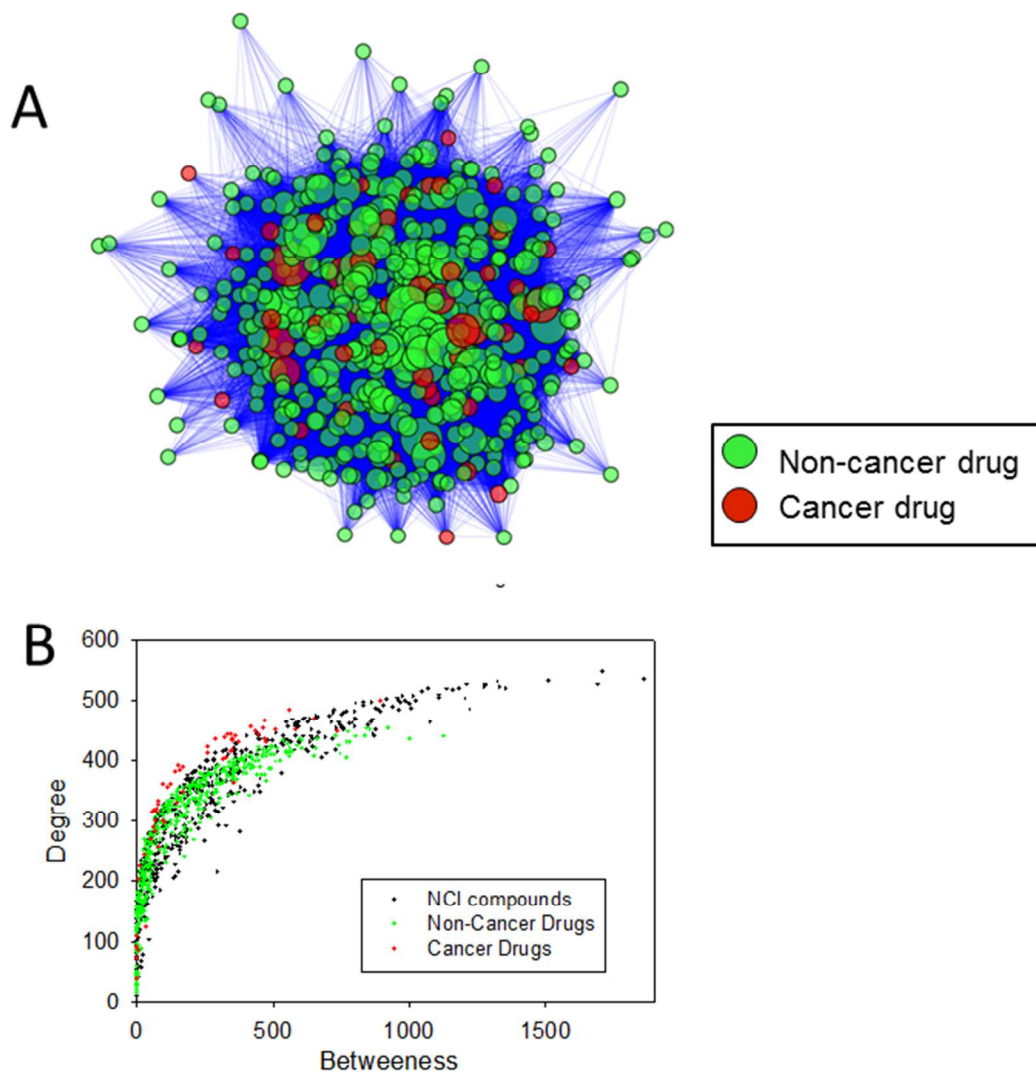


Figure 4

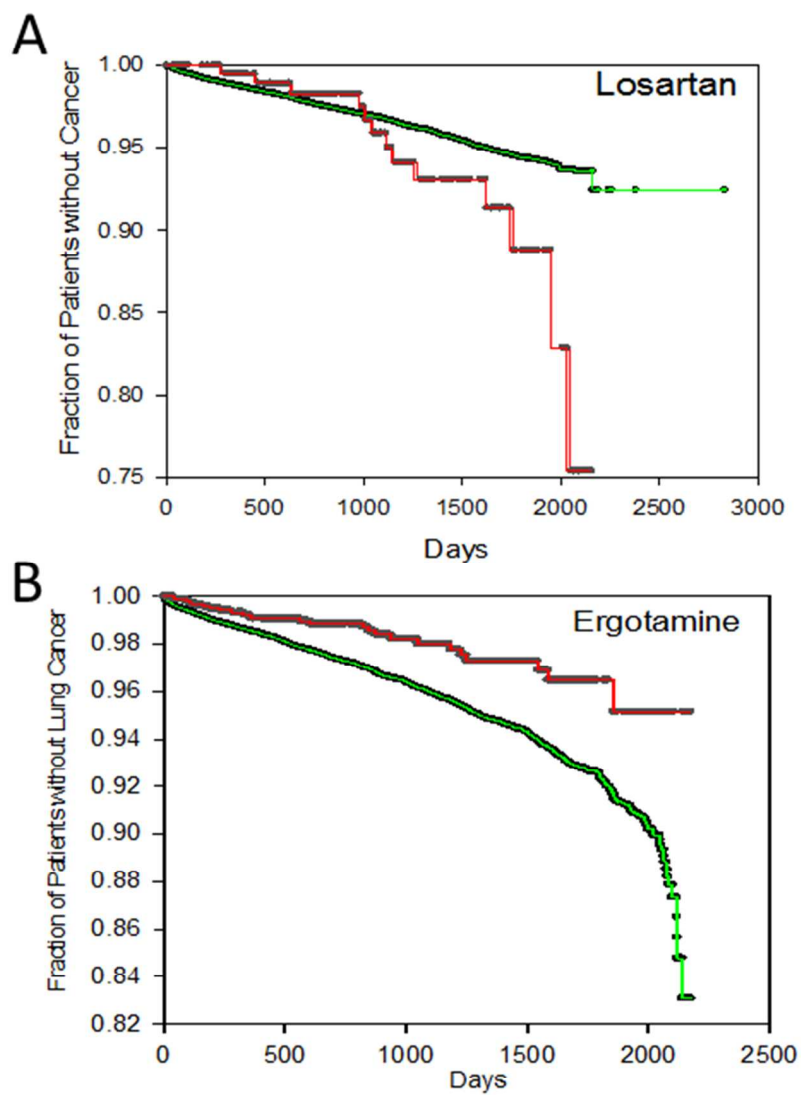
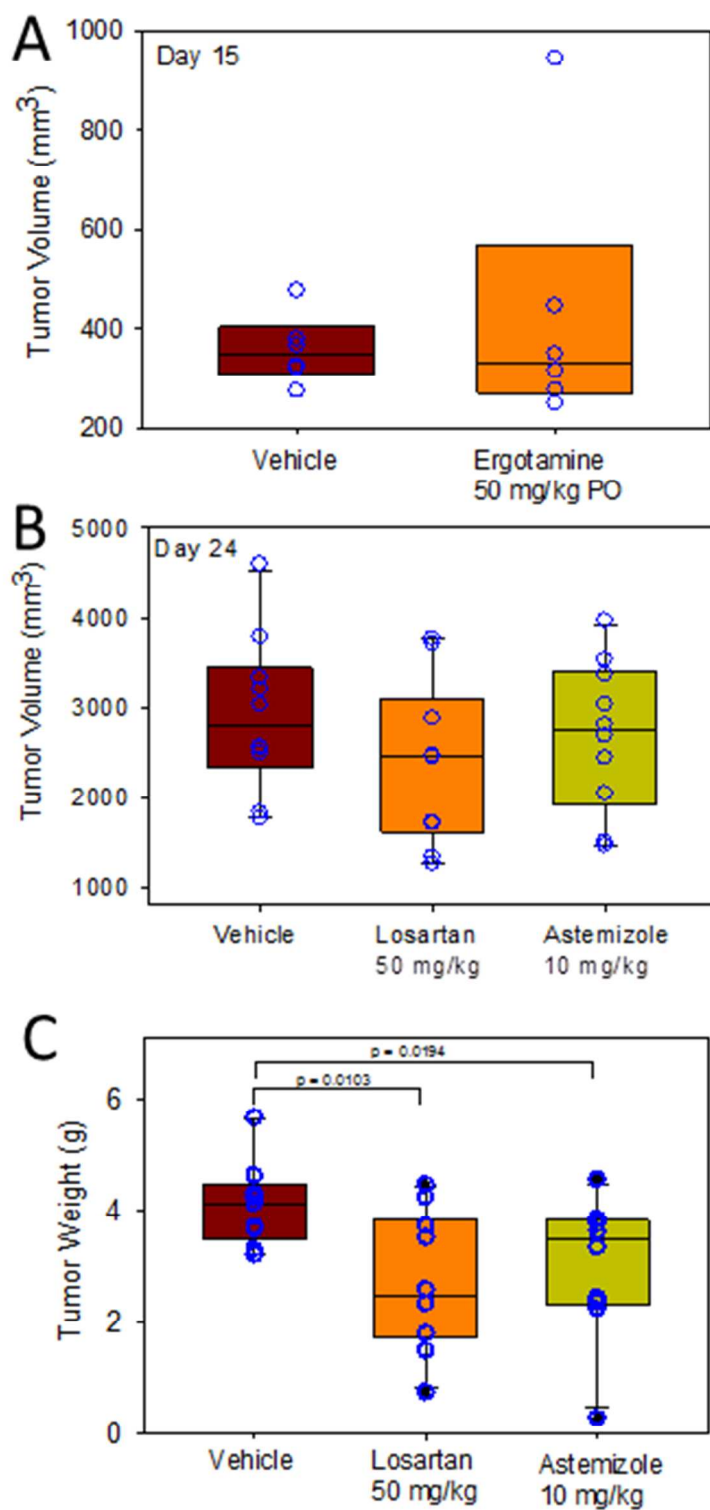


Figure 5



REFERENCES

1. W. Lee, Z. Jiang, J. Liu, P. M. Haverty, Y. Guan, J. Stinson, P. Yue, Y. Zhang, K. P. Pant, D. Bhatt, C. Ha, S. Johnson, M. I. Kennemer, S. Mohan, I. Nazarenko, C. Watanabe, A. B. Sparks, D. S. Shames, R. Gentleman, F. J. de Sauvage, H. Stern, A. Pandita, D. G. Ballinger, R. Drmanac, Z. Modrusan, S. Seshagiri and Z. Zhang, *Nature*, 2010, **465**, 473-477.
2. S. Jones, X. Zhang, D. W. Parsons, J. C. Lin, R. J. Leary, P. Angenendt, P. Mankoo, H. Carter, H. Kamiyama, A. Jimeno, S. M. Hong, B. Fu, M. T. Lin, E. S. Calhoun, M. Kamiyama, K. Walter, T. Nikolskaya, Y. Nikolsky, J. Hartigan, D. R. Smith, M. Hidalgo, S. D. Leach, A. P. Klein, E. M. Jaffee, M. Goggins, A. Maitra, C. Iacobuzio-Donahue, J. R. Eshleman, S. E. Kern, R. H. Hruban, R. Karchin, N. Papadopoulos, G. Parmigiani, B. Vogelstein, V. E. Velculescu and K. W. Kinzler, *Science*, 2008, **321**, 1801-1806.
3. T. Sjoblom, S. Jones, L. D. Wood, D. W. Parsons, J. Lin, T. D. Barber, D. Mandelker, R. J. Leary, J. Ptak, N. Silliman, S. Szabo, P. Buckhaults, C. Farrell, P. Meeh, S. D. Markowitz, J. Willis, D. Dawson, J. K. Willson, A. F. Gazdar, J. Hartigan, L. Wu, C. Liu, G. Parmigiani, B. H. Park, K. E. Bachman, N. Papadopoulos, B. Vogelstein, K. W. Kinzler and V. E. Velculescu, *Science*, 2006, **314**, 268-274.
4. D. W. Parsons, S. Jones, X. Zhang, J. C. Lin, R. J. Leary, P. Angenendt, P. Mankoo, H. Carter, I. M. Siu, G. L. Gallia, A. Olivi, R. McLendon, B. A. Rasheed, S. Keir, T. Nikolskaya, Y. Nikolsky, D. A. Busam, H. Tekleab, L. A. Diaz, Jr., J. Hartigan, D. R. Smith, R. L. Strausberg, S. K. Marie, S. M. Shinjo, H. Yan, G. J. Riggins, D. D. Bigner, R. Karchin, N. Papadopoulos, G. Parmigiani, B. Vogelstein, V. E. Velculescu and K. W. Kinzler, *Science*, 2008, **321**, 1807-1812.
5. L. D. Wood, D. W. Parsons, S. Jones, J. Lin, T. Sjoblom, R. J. Leary, D. Shen, S. M. Boca, T. Barber, J. Ptak, N. Silliman, S. Szabo, Z. Dezso, V. Ustyanksky, T. Nikolskaya, Y. Nikolsky, R. Karchin, P. A. Wilson, J. S. Kaminker, Z. Zhang, R. Croshaw, J. Willis, D. Dawson, M. Shipitsin, J. K. Willson, S. Sukumar, K. Polyak, B. H. Park, C. L. Pethiyagoda, P. V. Pant, D. G. Ballinger, A. B. Sparks, J. Hartigan, D. R. Smith, E. Suh, N. Papadopoulos, P. Buckhaults, S. D. Markowitz, G. Parmigiani, K. W. Kinzler, V. E. Velculescu and B. Vogelstein, *Science*, 2007, **318**, 1108-1113.
6. L. Ding, G. Getz, D. A. Wheeler, E. R. Mardis, M. D. McLellan, K. Cibulskis, C. Sougnez, H. Greulich, D. M. Muzny, M. B. Morgan, L. Fulton, R. S. Fulton, Q. Zhang, M. C. Wendl, M. S. Lawrence, D. E. Larson, K. Chen, D. J. Dooling, A. Sabo, A. C. Hawes, H. Shen, S. N. Jhangiani, L. R. Lewis, O. Hall, Y. Zhu, T. Mathew, Y. Ren, J. Yao, S. E. Scherer, K. Clerc, G. A. Metcalf, B. Ng, A. Milosavljevic, M. L. Gonzalez-Garay, J. R. Osborne, R. Meyer, X. Shi, Y. Tang, D. C. Koboldt, L. Lin, R. Abbott, T. L. Miner, C. Pohl, G. Fewell, C. Haipek, H. Schmidt, B. H. Dunford-Shore, A. Kraja, S. D. Crosby, C. S. Sawyer, T. Vickery, S. Sander, J. Robinson, W. Winckler, J. Baldwin, L. R. Chirieac, A. Dutt, T. Fennell, M. Hanna, B. E. Johnson, R. C. Onofrio, R. K. Thomas, G. Tonon, B. A. Weir, X. Zhao, L. Ziaugra, M. C. Zody, T. Giordano, M. B. Orringer, J. A. Roth, M. R. Spitz, Wistuba, II, B. Ozenberger, P. J. Good, A. C. Chang, D. G. Beer, M. A. Watson, M. Ladanyi, S. Broderick, A. Yoshizawa, W. D. Travis, W. Pao, M. A. Province, G. M. Weinstock, H. E. Varmus, S. B. Gabriel, E. S. Lander, R. A. Gibbs, M. Meyerson and R. K. Wilson, *Nature*, 2008, **455**, 1069-1075.
7. A. L. Hopkins, *Nat Chem Biol*, 2008, **4**, 682-690.

8. G. V. Paolini, R. H. Shapland, W. P. van Hoorn, J. S. Mason and A. L. Hopkins, *Nat Biotechnol*, 2006, **24**, 805-815.
9. L. Li, K. Bum-Erdene, P. H. Baenziger, J. J. Rosen, J. R. Hemmert, J. A. Nellis, M. E. Pierce and S. O. Meroueh, *Nucleic acids research*, 2010, **38**, D765-773.
10. L. Li, J. Li, M. Khanna, I. Jo, J. P. Baird and S. O. Meroueh, *ACS Med Chem Lett*, 2010, **1**, 229-233.
11. F. A. Shepherd, J. Rodrigues Pereira, T. Ciuleanu, E. H. Tan, V. Hirsh, S. Thongprasert, D. Campos, S. Maoleekoonpiroj, M. Smylie and R. Martins, *New Engl J Med*, 2005, **353**, 123-132.
12. S. Schmitt, D. Kuhn and G. Klebe, *Journal of molecular biology*, 2002, **323**, 387-406.
13. A. L. Hopkins, J. S. Mason and J. P. Overington, *Curr Opin Struct Biol*, 2006, **16**, 127-136.
14. J. Sangster, *European Journal of Medicinal Chemistry*, 1997, **32**, 842-842.
15. R. Wang, Y. Lu, X. Fang and S. Wang, *J Chem Inf Comp Sci*, 2004, **44**, 2114-2125.
16. P. Ferrara, H. Gohlke, D. J. Price, G. Klebe and C. L. Brooks, *J. Med. Chem.*, 2004, **47**, 3032-3047.
17. O. E. Brodde, *Pharmacology & therapeutics*, 2008, **117**, 1-29.
18. H. P. S. Wong, J. W. C. Ho, M. W. L. Koo, L. Yu, W. K. K. Wu, E. K. Y. Lam, E. K. K. Tai, J. K. S. Ko, V. Y. Shin and K. M. Chu, *Life sciences*, 2011, **88**, 1108-1112.
19. P. I. D'URSO, O. F. D'URSO, C. Storelli, M. Mallardo, C. DAMIANO GIANFREDA, A. Montinaro, A. Cimmino, C. Pietro and S. Marsigliante, *International journal of oncology*, 2012, **41**, 228-234.
20. J. T. Cross, E. M. Poole and C. M. Ulrich, *The pharmacogenomics journal*, 2008, **8**, 237-247.
21. M. A. Yildirim, K. I. Goh, M. E. Cusick, A. L. Barabasi and M. Vidal, *Nature Biotechnology*, 2007, **25**, 1119-1126.
22. K. H. Dragnev, W. J. Petty, S. J. Shah, L. D. Lewis, C. C. Black, V. Memoli, W. C. Nugent, T. Hermann, A. Negro-Vilar, J. R. Rigas and E. Dmitrovsky, *Clin Cancer Res*, 2007, **13**, 1794-1800.
23. M. A. Yildirim, K. I. Goh, M. E. Cusick, A. L. Barabasi and M. Vidal, *Nat Biotechnol*, 2007, **25**, 1119-1126.
24. P. Clark and B. Cottier, The activity of 10-, 14-, and 21-day schedules of single-agent etoposide in previously untreated patients with extensive small cell lung cancer, 1992.
25. L. Azoulay, T. L. Assimes, H. Yin, D. B. Bartels, E. L. Schiffrin and S. Suissa, *PloS one*, 2012, **7**, e50893.
26. W. Ahmed, M. Rahmani, P. Dent and S. Grant, *Cell Cycle*, 2004, **3**, 1305-1311.
27. E. Pasquier, S. Honore, B. Pourroy, M. A. Jordan, M. Lehmann, C. Briand and D. Braguer, *Cancer Res*, 2005, **65**, 2433-2440.
28. L. Li, J. Li, M. Khanna, I. Jo, J. P. Baird and S. O. Meroueh, *ACS. Med. Chem. Lett.*, 2010, **1**, 229-233.
29. D. S. Wishart, C. Knox, A. C. Guo, D. Cheng, S. Shrivastava, D. Tzur, B. Gautam and M. Hassanali, *Nucleic acids research*, 2008, **36**, D901-906.
30. Y. J. Huang, D. Hang, L. J. Lu, L. Tong, M. B. Gerstein and G. T. Montelione, *Mol Cell Proteomics*, 2008, **7**, 2048-2060.
31. D. S. Wishart, C. Knox, A. C. Guo, S. Shrivastava, M. Hassanali, P. Stothard, Z. Chang and J. Woolsey, *Nucleic acids research*, 2006, **34**, D668-672.

32. J. M. Word, S. C. Lovell, J. S. Richardson and D. C. Richardson, *J Mol Biol*, 1999, **285**, 1735-1747.
33. M. F. Sanner, *J Mol Graph Model*, 1999, **17**, 57-61.
34. M. Hendlich, A. Bergner, J. Gunther and G. Klebe, *J. Mol. Biol.*, 2003, **326**, 607-620.
35. A. Bergner, J. Gunther, M. Hendlich, G. Klebe and M. Verdonk, *Biopolymers*, 2001, **61**, 99-110.
36. J. J. Irwin and B. K. Shoichet, *J Chem Inf Model*, 2005, **45**, 177-182.
37. M. D. Eldridge, C. W. Murray, T. R. Auton, G. V. Paolini and R. P. Mee, *J Comput Aid Mol Des*, 1997, **11**, 425-445.
38. G. Jones and P. Willett, *Curr Opin Biotechnol*, 1995, **6**, 652-656.
39. D. R. Flower, *Journal of molecular graphics & modelling*, 1998, **16**, 239-253, 264.
40. J. M. Overhage, P. B. Ryan, C. G. Reich, A. G. Hartzema and P. E. Stang, *Journal of the American Medical Informatics Association*, 2012, **19**, 54-60.
41. P. E. Stang, P. B. Ryan, J. A. Racoosin, J. M. Overhage, A. G. Hartzema, C. Reich, E. Welebob, T. Scarnecchia and J. Woodcock, *Annals of internal medicine*, 2010, **153**, 600.
42. C. J. McDonald, J. M. Overhage, M. Barnes, G. Schadow, L. Blevins, P. R. Dexter and B. Mamlin, *Health Affairs*, 2005, **24**, 1214-1220.
43. P. Ryan, D. Griffin and C. Reich, 2009.